International Workshop

Unlocking the opening processes of the South China Sea

Tongji University, Shanghai. January 31-February 01, 2012.

Reference Materials

To facilitate discussions in the workshop, some basic information about the South China Sea is provided here.

The South China Sea--- Major features and basic information

Mostly based on

P. Wang & Q. Li (Eds.), 2009, *The South China Sea – Paleoceanography and Sedimentology*. Springer, 506p.

Li C.-F., Song T.-R., 2012, *Magnetic recording of the Cenozoic oceanic crustal accretion and evolution of the South China Sea basin*. Chinese Science Bulletin, in press.

1. Topography

The South China Sea (SCS) embracing an area of about $3.5x10^6$ km^2, being the largest marginal seas separating Asia from the Pacific. The bathymetry of the SCS comprises three parts: the deep basin, the continental slope and the continental shelf, respectively covering about 15%, 38% and 47% of the total area with an average water depth of about 1,140m. The major feature of the SCS topography is the rhomboid deep basin, which overlies oceanic crust and extends from NE to SW (Fig. 1). Water depth in the deep basin averages ~4, 700m, with a maximum depth of 5,559 m reported from its eastern margin yet to be confirmed by survey. The deep basin is divided by a chain of sea mounts along 15°N, or "Central Ridge", into two sectors: a relatively shallower northeastern part, and a deeper southwestern part (Wang Y. 1996).

The central deep basin is surrounded by continental and island slopes, topographically dissected and often studded with coral reefs. The northern slope with Dongsha reef island and the western slope with Xisha (Paracel Islands) and Zhongsha reefs (Macclesfield Bank) are separated by the Xisha Trough, while the southern slope is occupied by the Nansha Islands (Spratly Islands), the largest reef area in the SCS. The Nansha Islands are scattered on a carbonate platform known as "Dangerous Grounds", covering a broad area of ~570, 000 km^2. The eastern slope is narrow and steep, bordered by the deep-water Luzon Trough and Manila Trench (Fig. 2).

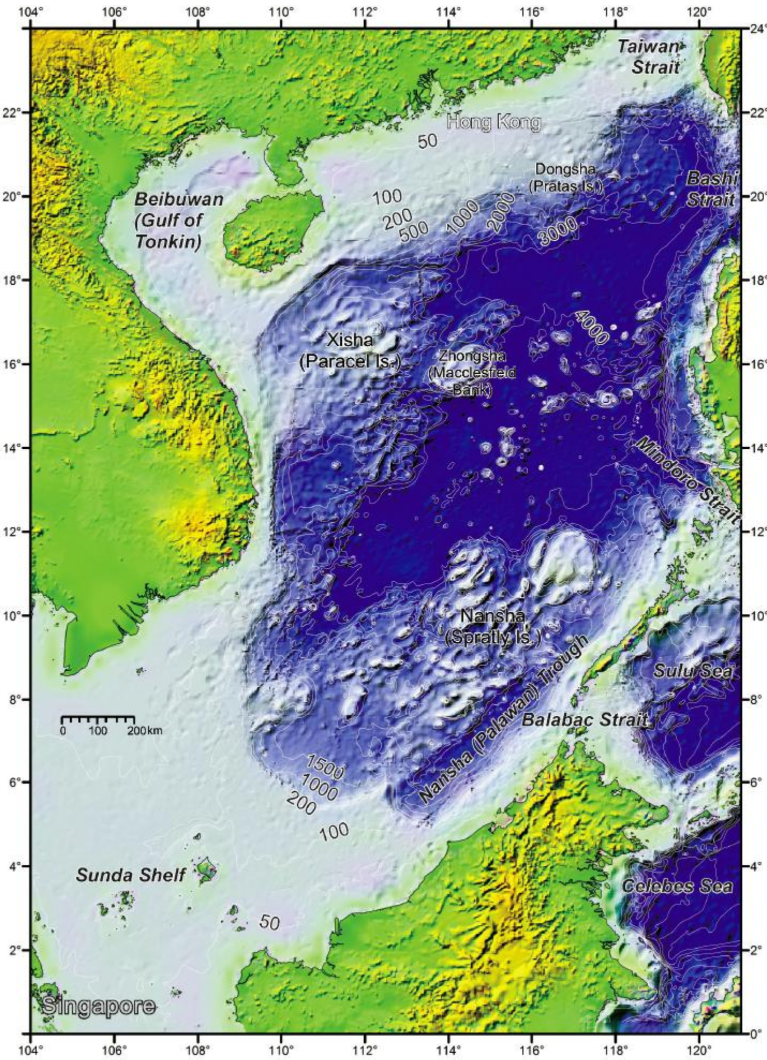

Fig. 1 Map shows the major topographic features of the South China Sea (SCS) and neighboring sea basins. Isobaths are in meters (m).

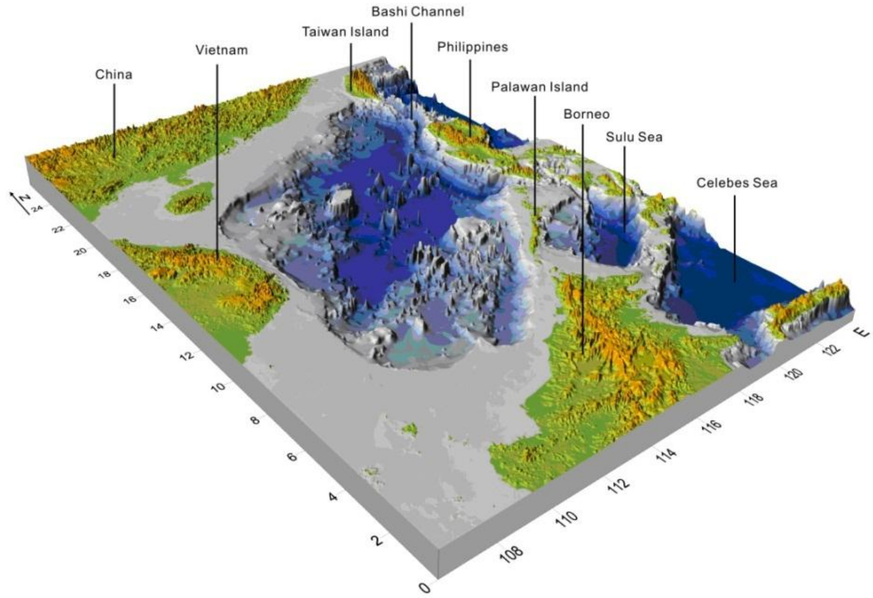

Fig. 2 Three-dimensional diagram shows the main geomorphologic feature of the SCS.

2. Sedimentary Basins

About 40 Cenozoic sedimentary basins or basin-groups have been recognized in the SCS (Fig. 2).

Rifting opened sedimentary basins of various depths and sizes that are often characterized by distinctive syn-rift and post-rift sediment packages. Three kinds of basins can be identified: those normal faulted often parallel to the coast, those sheared often controlled by major lateral-strike or transverse fault zones, and those compressional often relating to subduction. The Yinggehai and Zengmu basins are deepest, with sediment fill of over 14 km, about half of which was induced by structural subsidence. Basin inversion is common in tectonically active regions since the late Miocene. In the north, faulting direction changed from NE-SW in the Miocene to ENE-WSW or NE-SW in the Pliocene to NE-SW in the Quaternary. Terrigenous clastic sediments are predominant in shelf-slope basins, while hemipelagic components increase down-slope to over 50% in the central deep basin.

Fig. 3 Map shows distribution of Cenozoic sedimentary basins in the SCS as compiled from various sources. Refer to Table 2.4 for basin names and their synonyms.

3. Hydrology

The oceanography of the upper water of the SCS is largely dictated by two factors: the underlying morphology of the enclosed basin, and the overlying atmospheric circulation especially the East Asian Monsoon.

Driven by East Asian monsoons, the surface circulation is characterized by seasonally alternating basin-scale gyres (Fig. 3). The seasonal reversal in circulation leads to seasonal contrast in sea surface temperature (SST) and salinity (SSS) patterns (Fig. 4).Water exchanges with the Pacific and CO_2 exchange with the atmosphere are also subject to remarkable seasonal variations.

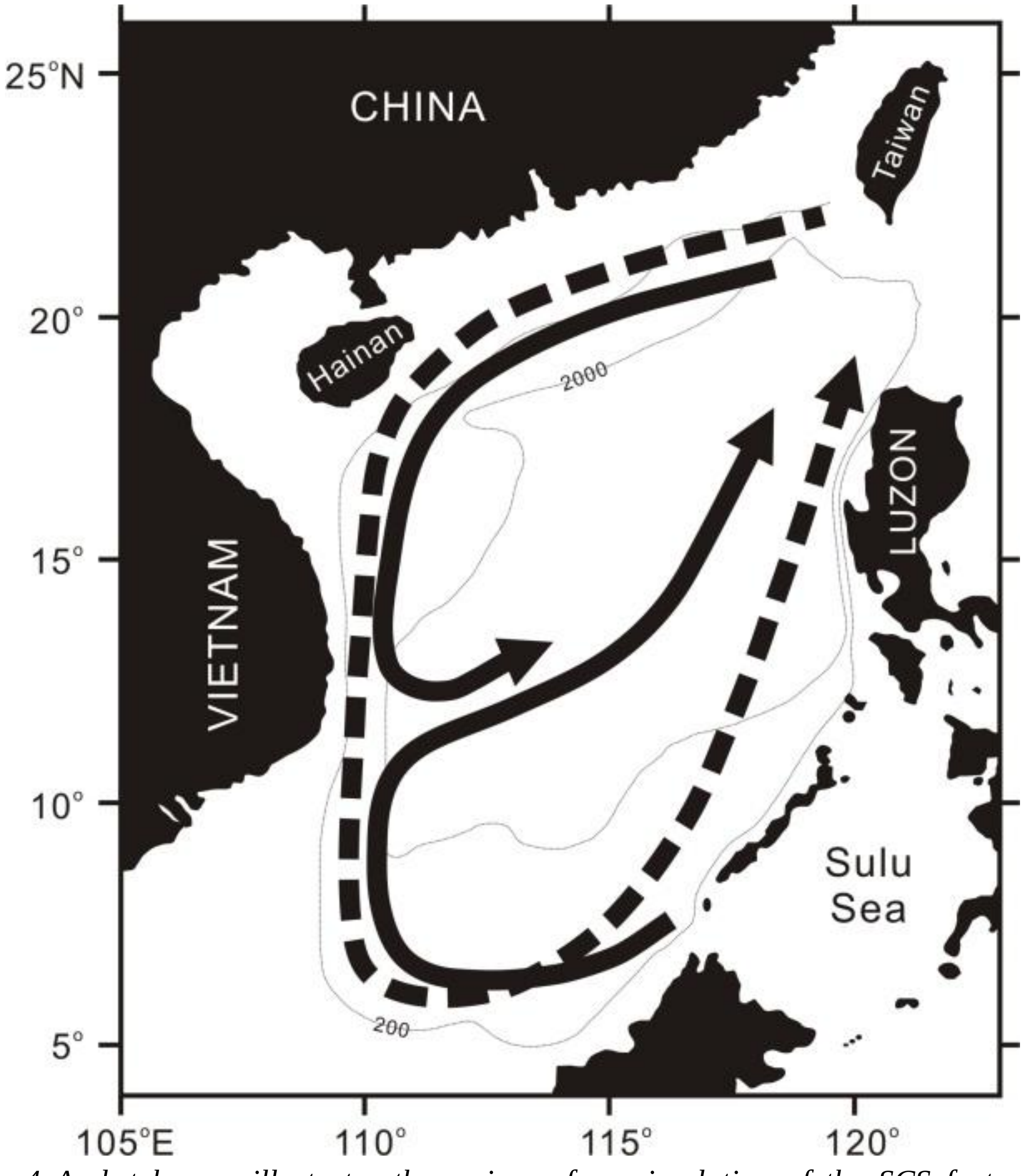

Fig. 4 A sketch map illustrates the main surface circulation of the SCS featuring seasonally alternating, basin-scale cyclonic gyres: winter (dashed line); summer (solid line). The summer pattern involves a cyclonic gyre in the northern and an anticyclonic gyre in the southern parts.

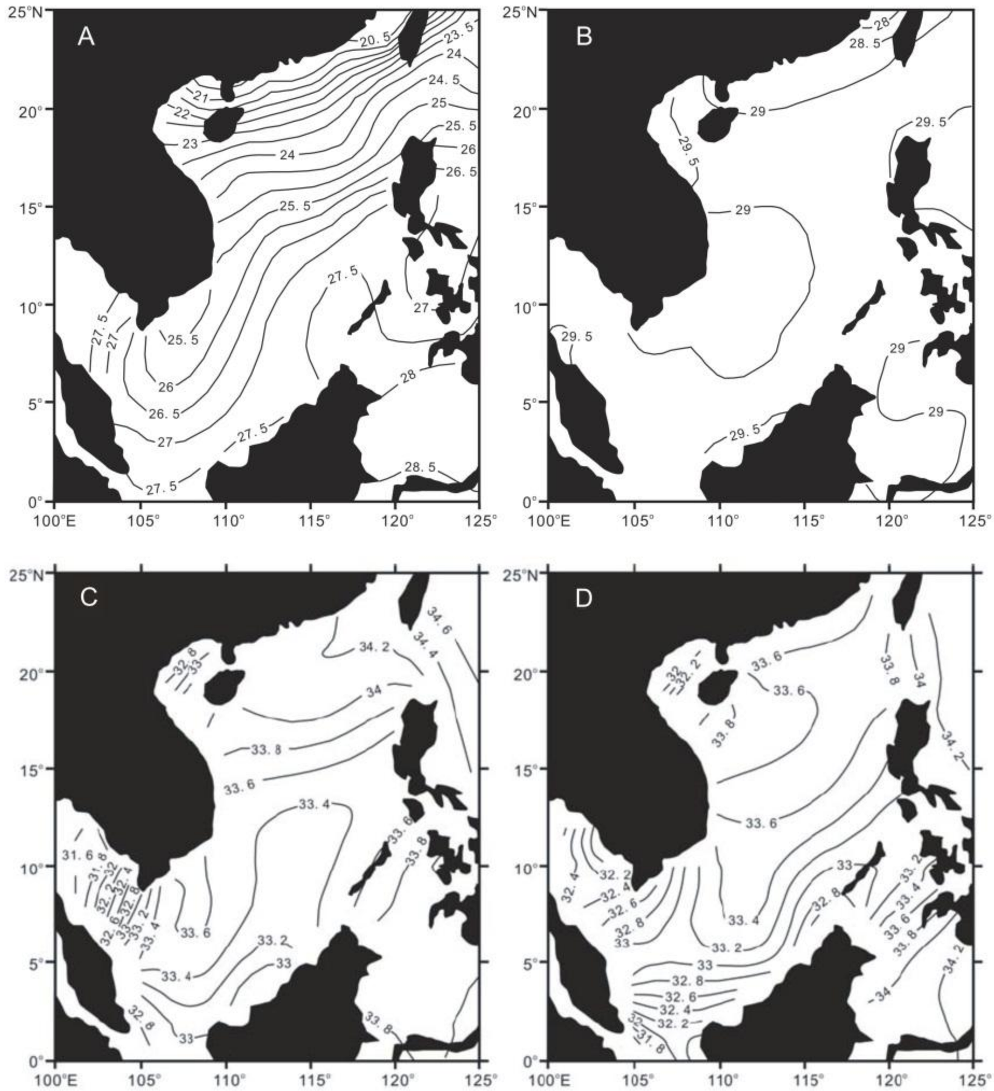

Fig. 5 Sea surface temperature (°C) and salinity (‰) in the modern SCS show distinct seasonality patterns: (A) SST in winter; (B) SST in summer; (C) SSS in winter; (D) SSS in summer.

The SCS basin is oceanographically dividable into two halves by the monsoon wind jet and the cross-basin current axis in a NE-SW direction, which is associated also with the upper layer thermohaline front. The northern part is controlled by the monsoon-driven cyclonic gyre, while the southern part belongs in the Western Pacific Warm Pool with much less monsoon influence.

Only the surface waters in the SCS exchange freely with those of the neighboring seas, while deeper waters flowing into the SCS are primarily from the western Philippone Sea through the Luzon (or Bashi) Strait (Fig. 5). The Luzon Strait transport has a sandwiched vertical structure, with the Philippine Sea water entering the SCS at the surface and in the deep ocean, and with the net Luzon Strait transport out of the SCS at the intermediate depth. Across the Luzon Strait, a persistent density difference exists between the Pacific and SCS. Water on the Pacific side is well stratified, but no deepwater stratification is obvious on the South China Sea side, where water density is vertically uniform with a density range of only about 0.02 kg /m^3 below 2000 m (Fig. 5).

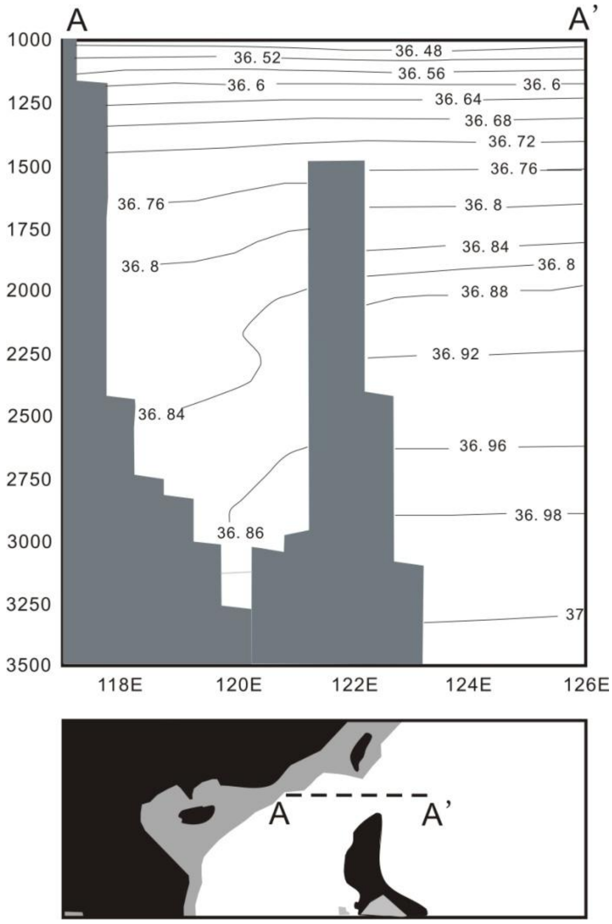

Fig. 6 Profile of potential density (kg /m^3) along 20°N, across the Luzon Strait (lower panel shows the location). Shading corresponds to bottom topography on the 0.5 ºgrid and does not indicate the deepest passages through Luzon Strait.

The deep water inflow in the SCS results in an estuarine basin-wide upwelling, a shorter residence time, and a shallower thermocline in the SCS than in the open ocean, making the upper water structure and productivity in the SCS more sensitive to monsoon variations.

Table 1 Major international geological cruises to the SCS since 1990.

Cruise	Time	Main topic	Reference
R/V Sonne, Germany			
SO 72a	Oct.25-Nov.18, 1990	Sedimentation	Wong, 1993
SO 95	Apr.12-Jun.05, 1994	Monitor Monsoon	Sarnthein et al.,1994
SO 114	Nov.20-Dec.12, 1996	Pinatubo ash	Wiesner et al., 1997
SO 115	Dec.13-Jan.16, 1997	Sunda Shelf	Stattegger et al., 1997
SO 132	Jun.17-Jul.09, 1998	Sedimentation	Wiesner et al., 1998
SO 140	Apr.03-May 04, 1999	Sedimentation	Wiesner et al., 1999
SO 177	Jun.02-Jul.02, 2004	Gas Hydrates	Suess et al.,
R/V JOIDES Resolution, USA			
ODP 184	Feb.11-Apr.12, 1999	Asian Monsoon	P.Wang et al., 2000
R/V Marion Dufresne, France			
MD106 (IMAGES III)	Apr.16-Jun.30, 1997	'IPHIS'	Chen et al., 1998
MD122 (IMAGES VII)	Apr.30-Jun.18, 2001	'WEPAMA'	Bassinot, 2002
MD147(IMAGES XII)	May 15-Jun.08,2005	' Marco Polo 1'	Laj et al., 2005

4. ODP Leg 184 & Other Cruises

Since the 1990s, numerous international expeditions were sent to the region to study topics ranging from climate and sea-level changes in Quaternary glacial cycles, monsoon evolution and variations, to volcanic ash distribution (Fig. 6, and Table 1). Of particular importance is the first paleoceanographic expedition, Sonne-95 cruise under the logo "Monitor Monsoon", which collected 48 piston and gravity cores at 46 sites from the SCS (Sarnthein et al. 1994) and revealed the regional late Quaternary paleoceanographic history for the first time (Sarnthein and Wang 1999). Paleoceanographic expeditions to the SCS were culminated with Ocean Drilling Program (ODP) Leg 184 in the spring of 1999, the first scientific deep-sea drilling expedition off the China coast. A total of 17 holes at 6 sites were cored on the southern and northern continental slopes of the SCS, to explore the late Cenozoic history of the East Asian monsoon (Wang P. et al. 2000). ODP Leg 184 provides the best deepwater stratigraphic sequence in the western Pacific, which archives evidence of the low-latitude oceanic response to orbital forcing (Wang P. et al. 2003c). The growing interest in SCS paleoceanography continues after the ODP cruise, as seen from the joint French-Chinese "Marco Polo" cruise to the SCS in 2005 (Laj et al. 2005) and several other Chinese and international cruises after 2005.

5. Stratigraphy

Over the last three decades, intensive industrial drilling and marine geological research climaxing with ODP Leg 184 have generated voluminous data on the variations and distribution of sediment sequences in the SCS. Seismic stratigraphy indicates a sediment cover of ~1 km in the SCS deep basin except in areas close to seamounts. The deepest hole so far drilled is at ODP Site 1148 in the lower slope of the northern SCS, at a water depth of 3,292 m. Hole 1148A penetrated to 853 m and recovered a 632 m sediment sequence (~74% core recovery), over the last ~33 Ma (Fig. 7).

The Oligocene section exceeds 390 m, about 90% of which, ~350 m, are monotonous grayish to olivergreen, quartz-rich clay that accumulated during the early Oligocene at a sedimentation rate of over 60 m/myr. This section is mixed between deep water and shallow water biofacies. The Oligocene/Miocene boundary coincides with the unconformity at the top of the slumped unit, and sediment-mixing due to slumps characterizes the upper Oligocene sediments that bracket the double seismic reflectors (Figure 8). This slumped unit and associated unconformities signal a large-scale tectonic transition from rifting to spreading probably relating to the ridge jump centered at about25 Ma. The missing section spans a time interval of about 3 myr although all the slumped sediment could have accumulated in a short time period.

The lower Miocene consists mainly of greenish to grayish brown nannofossil clay mixed sediments, with common iron sulfide particles. Due to a greater water depth at the site, biogenous skeletons are strongly affected by dissolution. A better preserved Miocene to Pliocene succession was recovered at the shallower northern Site 1146 (2,092 m) and southern Site 1143 (2,772 m) with oldest sediments of 18.6 Ma and ~11 Ma, respectively. Unlike those from the north, the late Miocene section at Site 1143 contains many thin turbidite layers), similar to those found in the Nansha (NW Borneo) Trough, offshore from

Sabah and Palawan.

Stratigraphic correlation has been advanced by astronomically tuned timescales based on isotopic records from ODP Site 1143 (Fig. 9) (Tian et al., 2002) and isotopic and magnetic records from ODP Site 1148 (Fig. 10) (Tian et al., 2008), which not only provide a more accurate standard for refining deep sea stratigraphy but also offer information useful for reconstructing the history of the SCS.

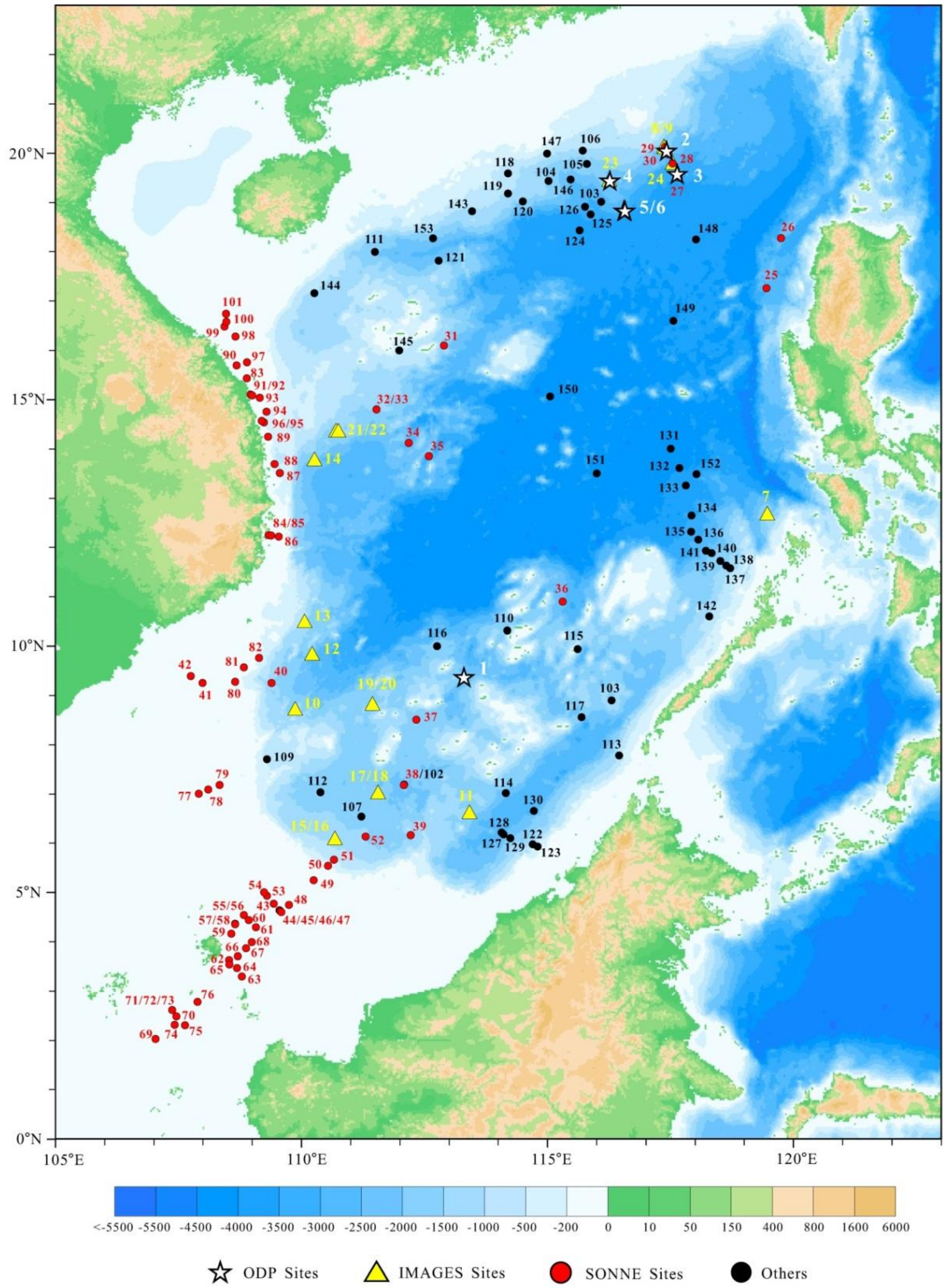

Fig. 7 Locations of cores collected for paleoceanographic studies up to 2005 in the South China Sea.

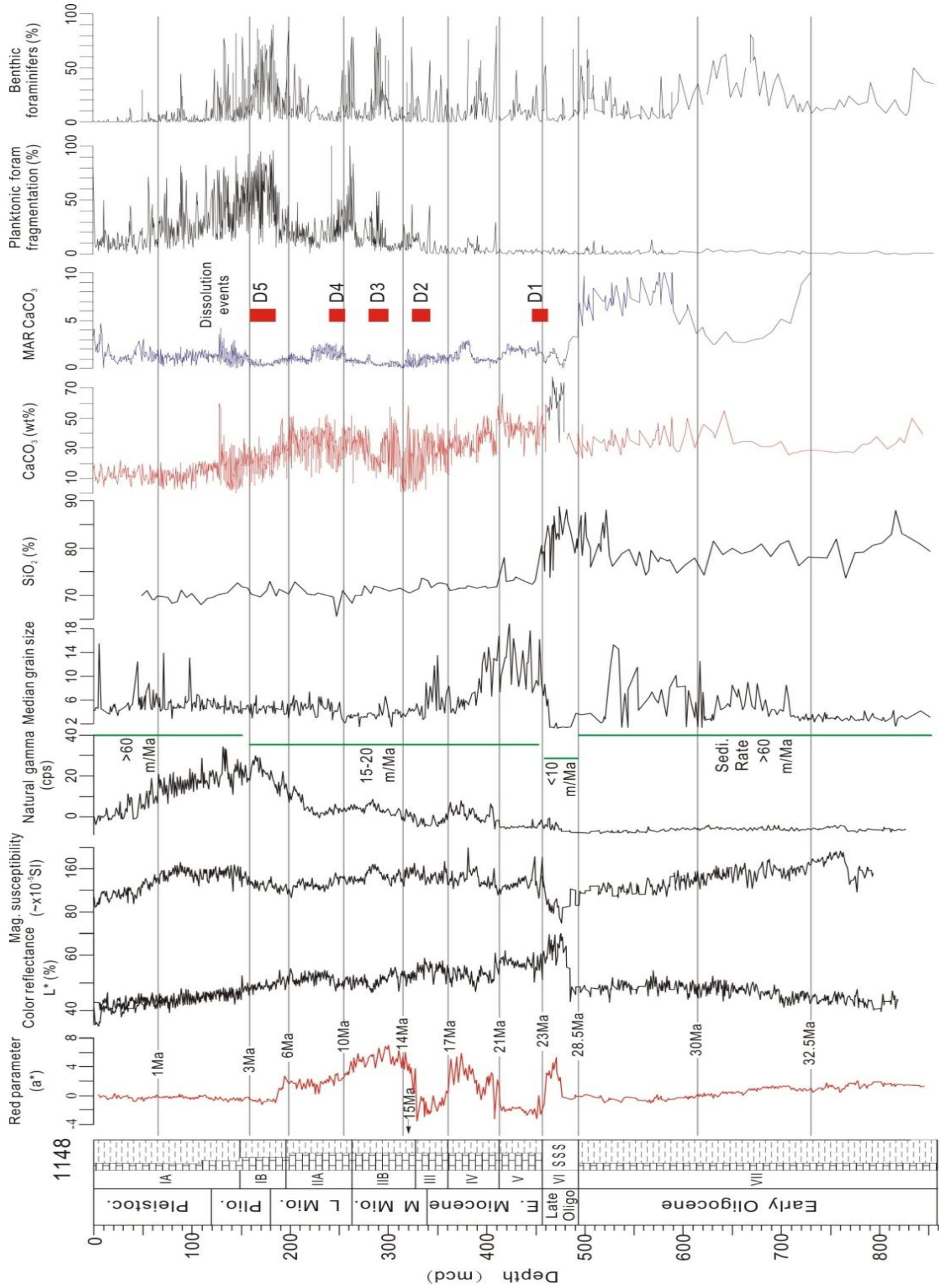

Fig. 8 Lithostratigraphic units, geophysical logs, major sediment components and foraminiferal features from ODP Site 1148.

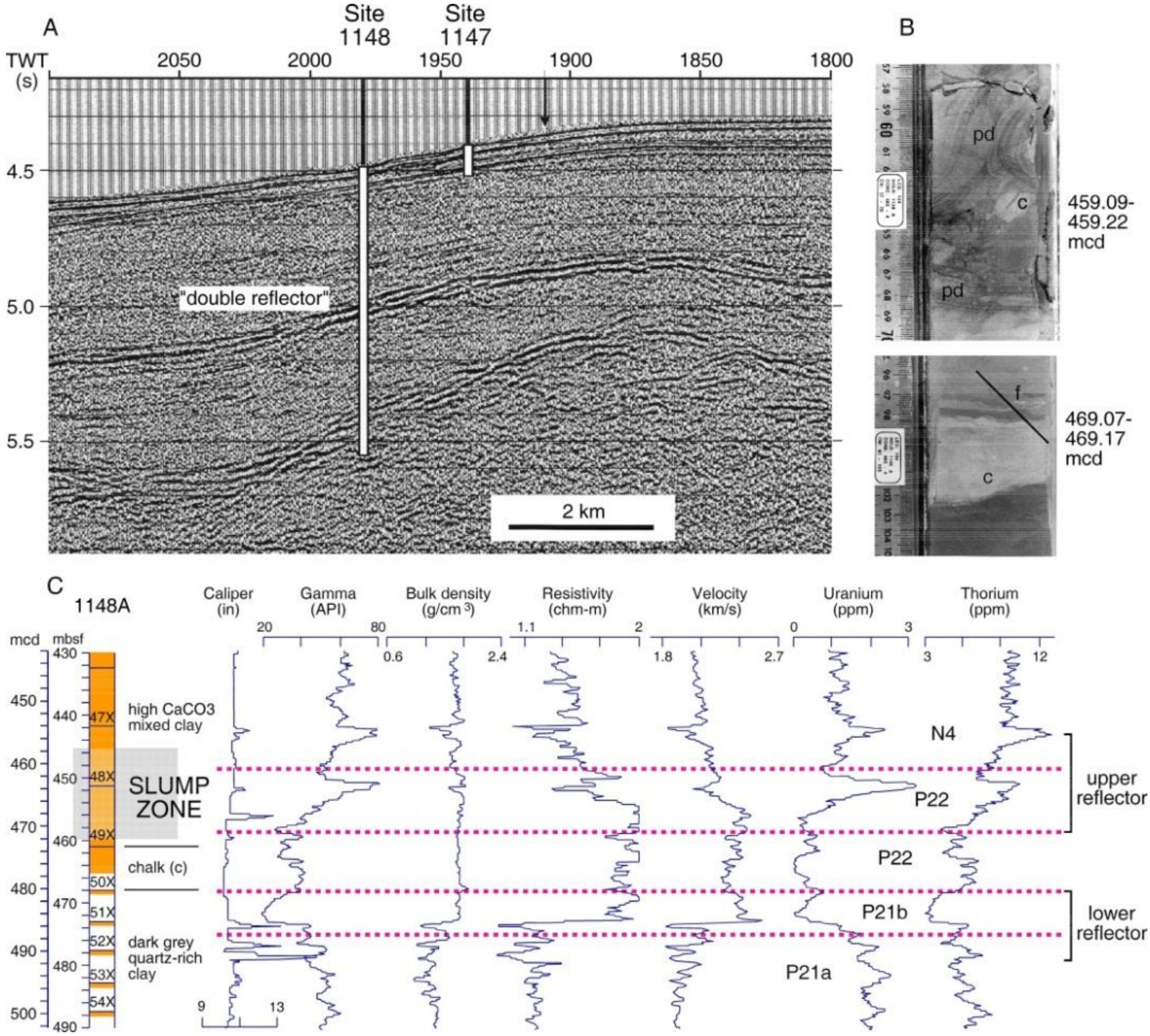

Fig. 9 Geophysical and lithological characteristics marking late Oligocene slumped deposits and unconformities at ODP Site 1148 are documented in (A) a double reflector (DR) on seismic profile, (B) core sediments showing displaced chalk (c), microfaults (f), and plastic deformation (pd), and (C) strong swings in all physical log readings. Dashed horizontal lines in C indicate unconformities defined by biostratigraphy, with planktonic foraminifer zones P21, P22 and N4 indicated

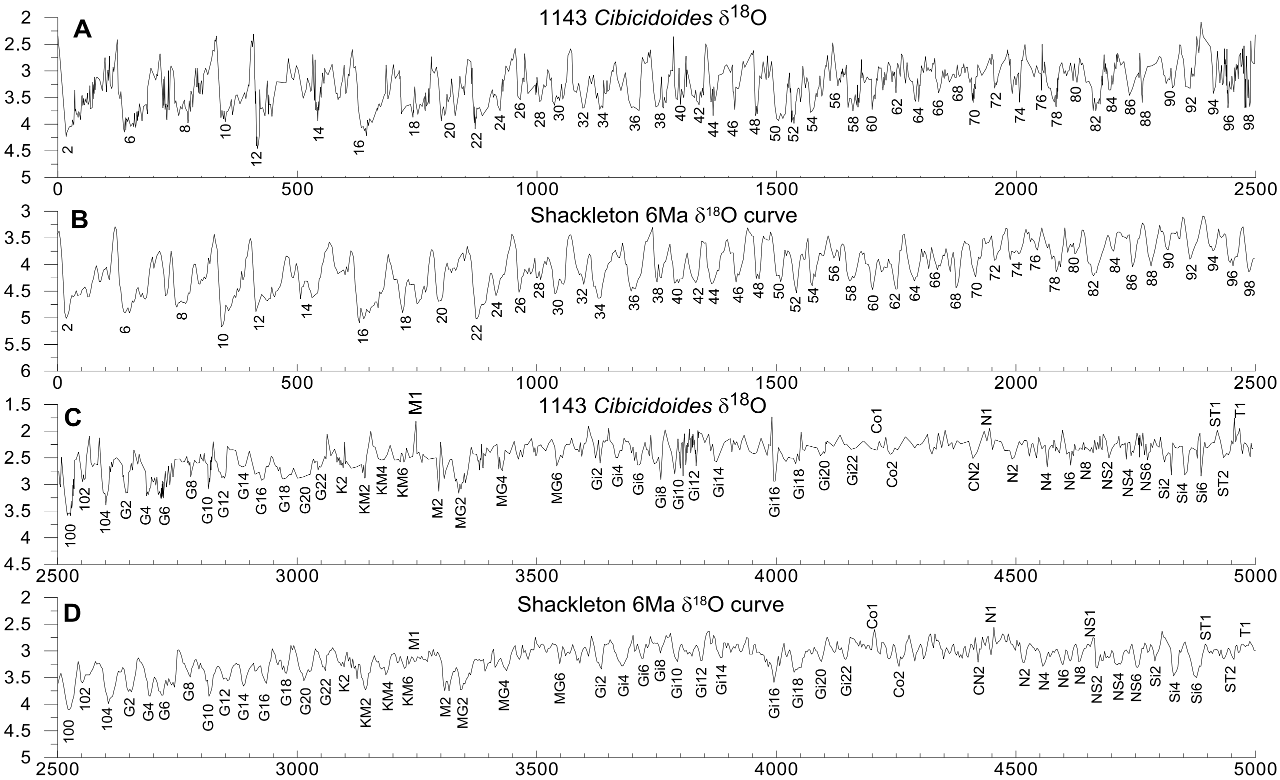

Fig. 10 Correlation of ODP 1143 $\delta^{18}O$ data with Shackleton's 6 myr composite $\delta^{18}O$ curve. Benthic foraminifer $\delta^{18}O$ curves from 0 to 2.5 myr : A. ODP 1143, B. composite $\delta^{18}O$ curve ; from 2.5 to 5.0 myr: C. ODP 1143, D. composed $\delta^{18}O$ curve.

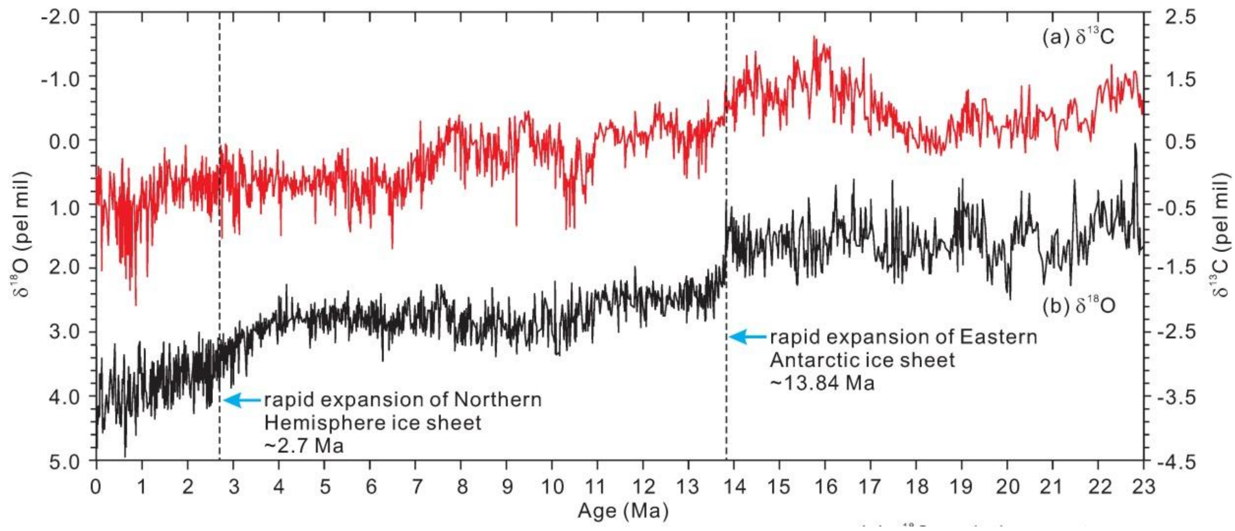

Fig. 11 Benthic foraminiferal isotopic $\delta^{13}C$ (red) and $\delta^{18}O$ (black) records of ODP Site 1148 (0–23 Ma).

6. Sedimentology

The South China Sea (SCS) receives approximately 700 million tons of deposits annually in modern times, including about 80% of terrigenous matters provided by surrounding rivers and 20% of biogenic carbonate and silicates and volcanic ash. A similar scenario has been indentified also in the geological past. Since the early Oligocene, the sea has accumulated about

14.4 thousand trillion tons of deposits, which contain 63% terrigenous matters and 37% biogenic carbonate with negligible biogenic silicates and volcanic materials. Most of these deposits accumulated on the SCS shelf (43% of total sediment mass) and slope (52%). Such a huge deposition cover makes the SCS an ideal place to study terrigenous input, paleoceanograhy, and regional and global climate evolution as well as sedimentary evolution of the SCS.

Two main source areas with markedly different geological characteristics contribute terrigenous sediments to the SCS. The northern and western source is mainly the Asian continent and Taiwan, while the southern and eastern source consists of islands or volcanic arcs lying along the eastern margin of the SCS (Figure 12). Weathering products from these land-source areas are transported to the SCS chiefly by larger rivers, mainly the Mekong River, Pearl River, and Red River, and small mountainous rivers especially those in southwestern Taiwan (Table 2). Here we characterize clay mineralogy and geochemistry of these source areas.

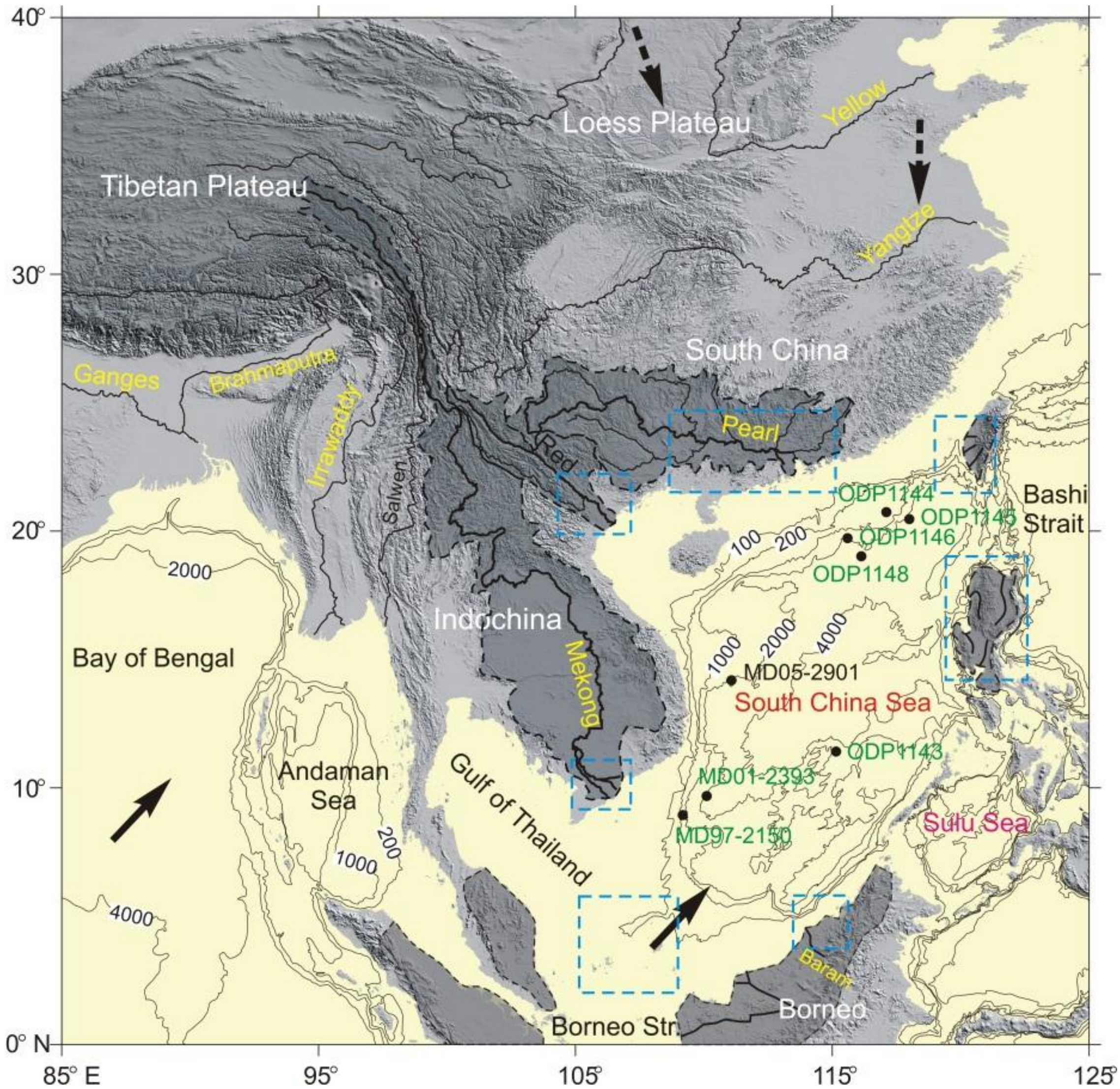

Fig. 12 Major river drainage basins surrounding the SCS, with dashed squares indicating sediment source areas and dots indicating locations of IMAGES cores and ODP Leg 184 sites. Also shown are prevailing wind flows during summer (solid arrows) and winter (dashed arrows).

Table 2. Drainage area, runoff, and suspended sediment discharge are listed for major rivers flowing directly into the SCS.

River	Drainage area (km^2)	Runoff (m/yr)	Suspended sediment discharge (Mt/yr)	Data source
Pearl (South China)	440,000	6.9	69.0	Milliman and Syvitski (1992)
Red (Vietnam)	120,000	10.0	130.0	
Mekong (Vietnam)	790,000	5.9	160.0	
Chao Phraya (Thailand)	160,000	1.9	11.0	
Ta-An (Taiwan)	633	1.6	7.1	Dadson et al. (2003)
Wu (Taiwan)	1,981	1.9	9.8	
Cho-Shui (Taiwan)	2,989	1.2	54.1	
Pei-Kang (Taiwan)	597	1.3	2.2	
Pa-Chang (Taiwan)	441	1.5	6.3	
Tseng-Wen (Taiwan)	1,157	1.1	25.1	
Erh-Jen (Taiwan)	175	1.8	30.2	
Kao-Ping (Taiwan)	3,067	2.5	49.0	
Tung-Kang (Taiwan)	175	2.9	0.4	
Lin-Pien (Taiwan)	310	2.5	3.3	
Baram (Malaysia)	22,800	2.5	12	Hiscott (2001), Lambiase et al. (2002)

The Cenozoic ocean has experienced significant decrease in carbonate compensation depth and carbon isotope value. When the 24-myr low-resolution carbonate MAR profile from Site 1148 in the northern SCS are compared with the stacked Neogene time series from western and central equatorial Pacific, remarkable differences emerge between the three curves (Fig. 13)

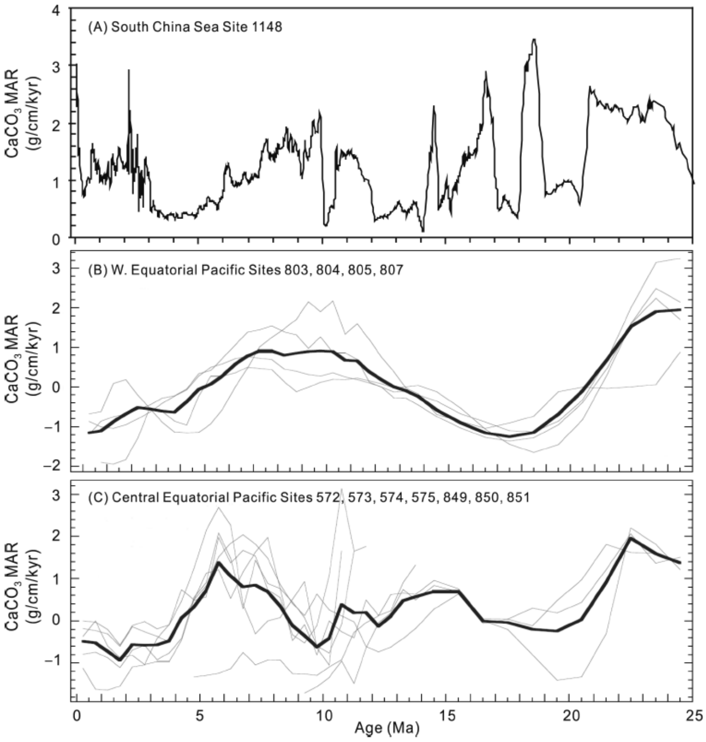

Fig. 13 Carbonate MAR time series from (A) Site 1148 from the SCS are compared to sites from (B) western and (C) central equatorial Pacific. The thick lines in D and E are stacks while the thin lines are time series.

In summary, the total deposit mass in the SCS from the beginning of seafloor spreading in the Oligocene is about 1.44×10^{16} t. Highest accumulation rates occurred in the Oligocene (~ 22 g $\cdot$ cm^{-2} $\cdot$ kyr^{-1}) and Quaternary (~ 15 g cm^{-2} kyr^{-1}), compared to relatively low accumulation rates (~ 10 g cm^{-2} ka^{-1}) in the Miocene-Pliocene. More than 80% of the SCS sediments were deposited in basins along its continental margin. Highest accumulation rates occur close to areas of active tectonics but not necessarily near large river mouths, indicating that uplift rate in the source area but not the drainage size has been critical in determining river discharge and sediment deposition. Sediment distribution patterns changed in different evolution stages of the SCS.

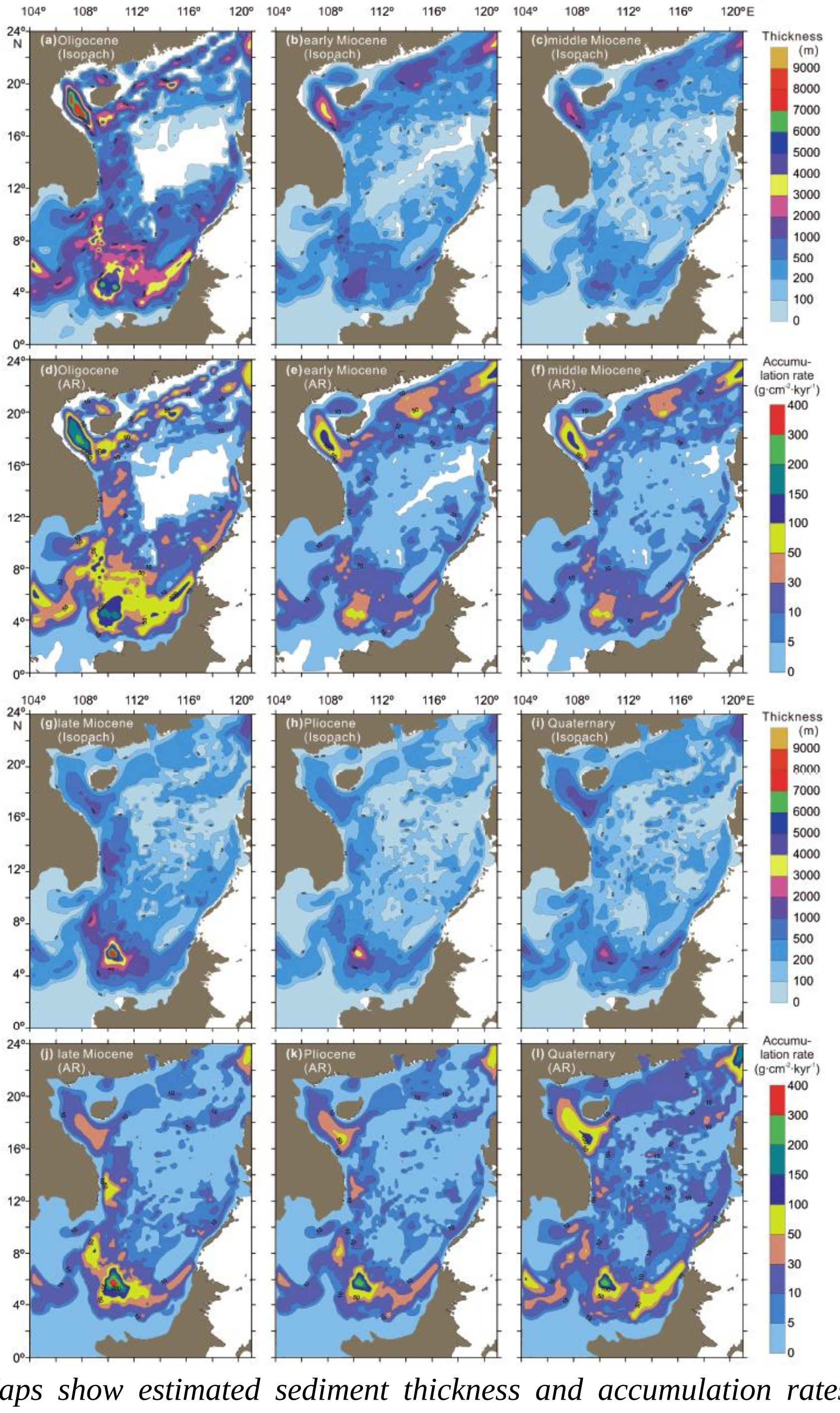

Fig. 14 Maps show estimated sediment thickness and accumulation rates (AR) in various periods.

7. Recent tectonic and geophysical synthesis

Precise calibration and characterization of the continent-ocean boundary (COB)

We define the continent-ocean boundary (COB) of the SCS through comprehensive analyses of gravimetric, magnetic and reflection seismic data (Fig. 15). It is found that the COB is well correlated to a transitional boundary in free-air gravity anomalies. The area floored with oceanic crust corresponds to an area of mostly positive free-air gravity anomalies, which is generally rimmed by areas or belts of negative free-air gravity anomalies. The transitional boundary from the grossly positive to negative gravity anomalies can define the COB.

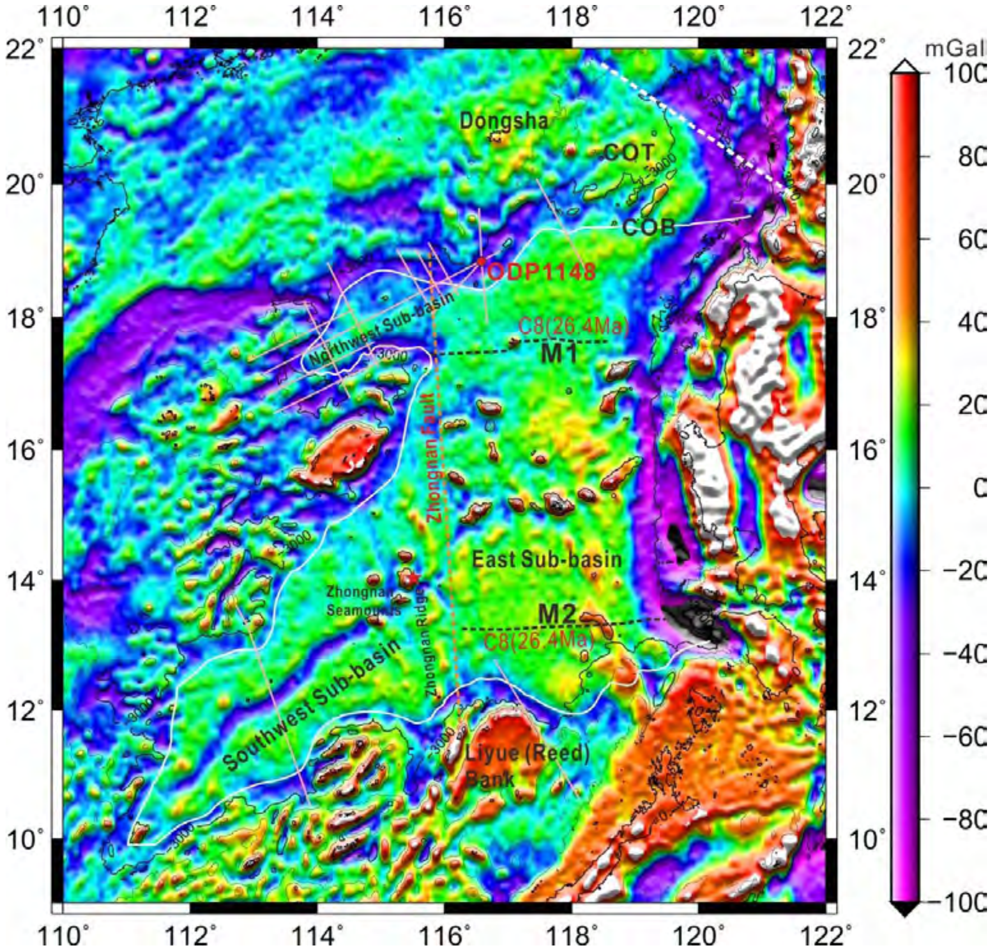

Figure 15 Free-air gravity anomaly map of the South China Sea (based on the 1-min grid). The light yellow solid lines are reflection seismic sections. The two bold black dashed lines mark the two magnetic anomalies M1 and M2 interpreted from Figure 16. The white solid line marks the interpreted COB. The red solid pentacle in the Zhongnan Seamounts marks the sampling site of alkaline basalts (K-Ar age: 3.49 Ma).

Recognizing the magnetic zonation in the SCS and revisiting the opening episodes of the SCS basin

With a 2D wavelength-domain cosine-tapered band-pass filter, we cut all wavelength components longer than 200 km and shorter than 10 km, and pass all wavelength components between 20 km and 100 km. This operation leads to more distinguishable magnetic anomalies caused by seafloor spreading (Figs. 16 and 17). We find that the oldest identifiable magnetic anomaly caused by seafloor spreading near the northern SCS continental margin is C12

(~32 Ma), but this anomaly is not identifiable near the southern continental margin. There are still large uncertainties in the opening ages of the Southwest Sub-basin, and we find that computed magnetic anomalies from two different age models can all fit observed anomalies reasonably well (Fig. 18). Thus presently available magnetic field data cannot help pinpoint exactly whether the Southwest and East Sub-basins opened simultaneously or in any sequential orders. However, models with a single episode of opening cannot explain the sharp tectonophysical differences across the Zhongnan Fault. Further studies on the spreading history and episode will have to incorporate regional reflection seismic data. High-resolution near-bottom magnetic surveys and deep ocean drilling will be critical to fully solving these problems in oceanic crustal ages and marginal sea evolutions. Patterns in magnetic zonation indicate that the age of magnetic anomalies M1 and M2 (C8, ~ 26 Ma) represents the timing of a key tectonic event during the opening of the SCS. This event could be associated with a change in seafloor spreading rates and/or regional magmatic activities in the SCS. The previously thought ridge jump after C7 in the east part of the South China Sea may not actually occur.

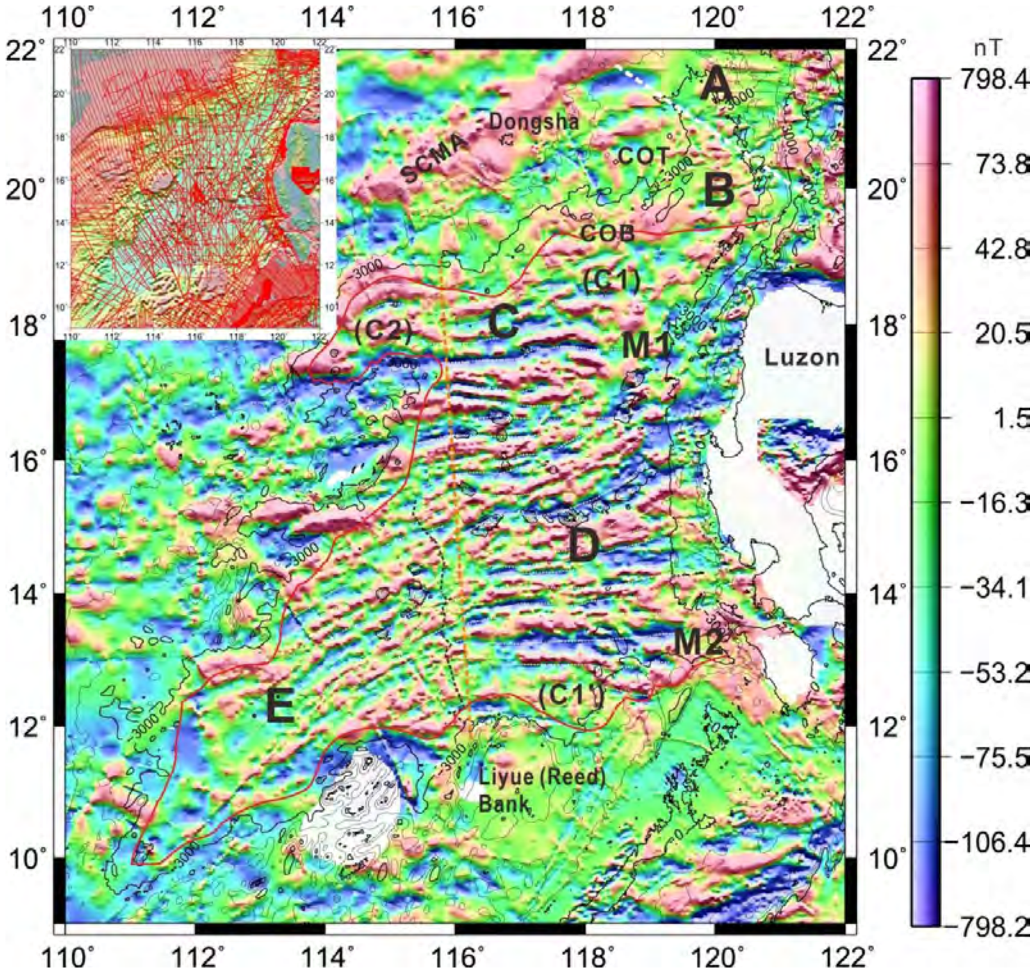

Figure 16 Total-field magnetic anomaly map of the South China Sea (SCS) showing magnetic zonation. A, B, C (C1, C1', C2), D, and E are different magnetic zones. M1 and M2 are major magnetic boundaries in the East Sub-basin, and their ages are estimated to be C8 (~ 26 Ma). The red solid line marks the continent-ocean boundary (COB). The light yellow dashed line marks the Zhongnan Fault. The black dashed line marks the Zhongnan Ridge. The white bold dashed line marks the Luzon-Ryukyu Transform Boundary (Shu et al., 2004). The white thin dashed lines are sketches of negative magnetic anomalies in the central basin. SCMA = offshore south China magnetic anomaly. The inlet in the upper left corner is the regional topography overlapped with magnetic tracks in red lines.

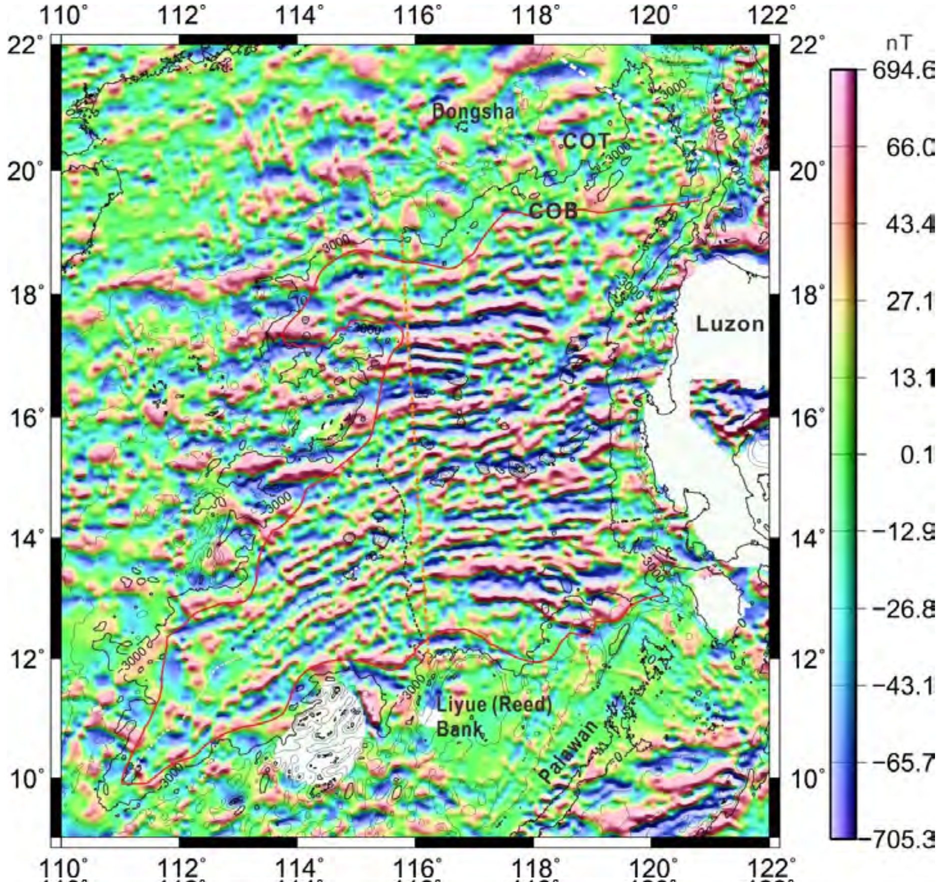

Figure 17 Total-field magnetic anomaly map of the South China Sea after the 2D wavenumber-domain filtering. The light yellow dashed line in the Southwest Sub-basin shows the track of the negative free-air gravity anomaly along the relict spreading center (Figure 1).

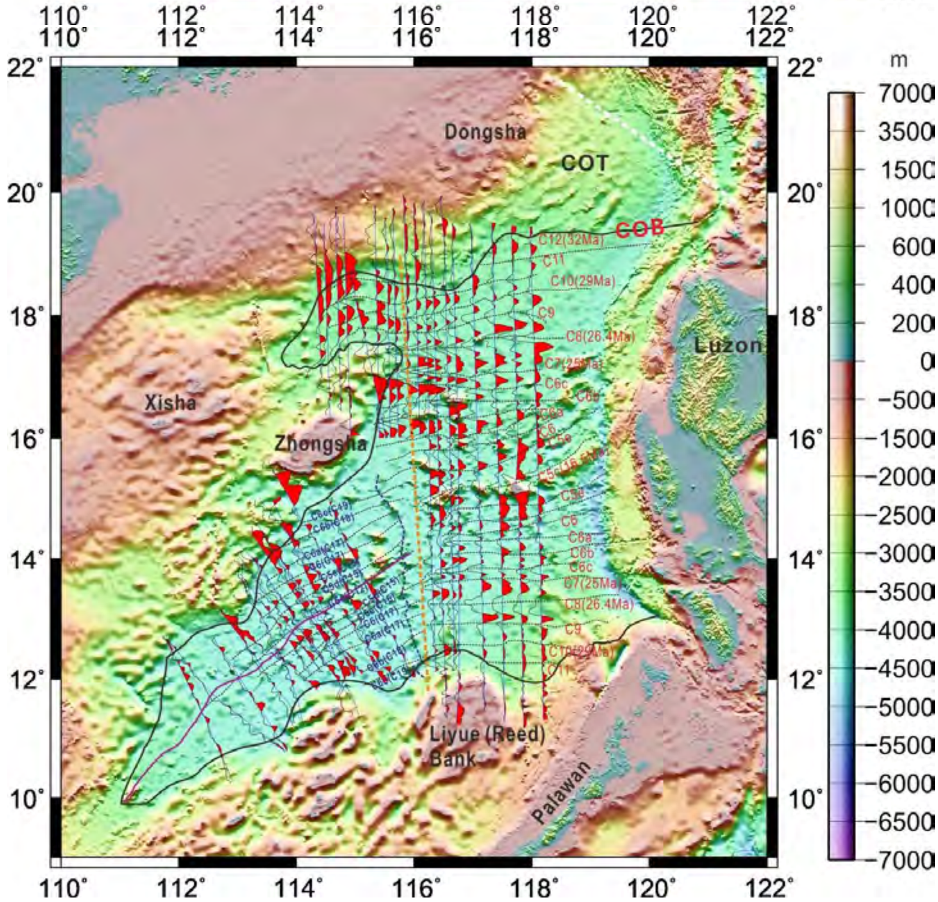

Figure 18 Bathymetry, key magnetic profiles, and interpreted ages and their spatial distributions [Song & Li, 2012]. The black thin dashed lines are sketches of interpreted negative magnetic anomalies in the central basin. Their preliminary ages are modeled based on the geomagnetic polarity time scales CK95 [Cande & Kent, 1995]. Two possible but different seafloor spreading models are shown in the Southwest Sub-basin. The purple solid line in the Southwest Sub-basin shows the track of the negative free-air gravity anomaly along the relict spreading center (Figure 15).

The Zhongnan Fault, Zhongnan Ridge and Zhongnan Seamounts

The Zhongnan Fault and Zhongnan Ridge (Figs. 15,16,17, and 18) are important tectonic units in the central SCS basin and reflect themselves well on geophysical fields. The Zhongnan Fault is the boundary between the East and Southwest Sub-basins; The Zhongnan Ridge shows a V-shaped apex and strong internal deformations on reflection seismic sections, and these features could be formed by compression along a fracture zone where strong hydrothermal activities could also develop. Around the Zhongnan Seamounts, both the Curie points and top of the magnetic layer are abnormally shallow, indicating deep active geothermal activities. These findings are conformable with very young magmatism discovered at the Zhongnan Seamounts, and they together suggest that strong late-stage magmatism occurred deep in the Southwest Sub-basin after the cessation of the seafloor spreading. Therefore, the anomalously higher surface heat flow in the Southwest Sub-basin than in the East Sub-basin is possibly linked to stronger late-stage magmatism there, and may not used directly in indicating that the oceanic crust of the Southwest Sub-basin is younger.

Deep magnetic layer structure and thermal evolution

The shallowest Curie points in the SCS basin are within the eastern part of the Southwest Sub-basin (Fig. 19), and this is known attributable to late-stage magmatism there. In the East Sub-basin, smallest Curie depths tend to occur mostly to the north than to the south of the relict spreading center, implying more intense deep geothermal activities to the north, which are also consistent to stronger late-stage seafloor volcanisms there.

Within the central basin where oceanic crust developed and in the COT of the northern SCS continental margin, Curie points are elevated, and the magnetic layer is appreciably thinner (mostly < 23 km) than in the surrounding areas (Figs. 20 and 21). A magnetized layer of about 10 km in thickness in the uppermost mantle is identified beneath the SCS, and it can contribute to near surface magnetic anomalies (Fig. 21). The regional air-borne and marine magnetic anomalies after filtering with low-pass filters of 300 km and 400 km cutoff wavelengths bear high similarities to satellite magnetic anomalies, again confirming that regional near surface magnetic anomalies contain true long-wavelength magnetic anomalies contributed by lower crust and upper mantle magnetic sources (Figs. 22 and 23).

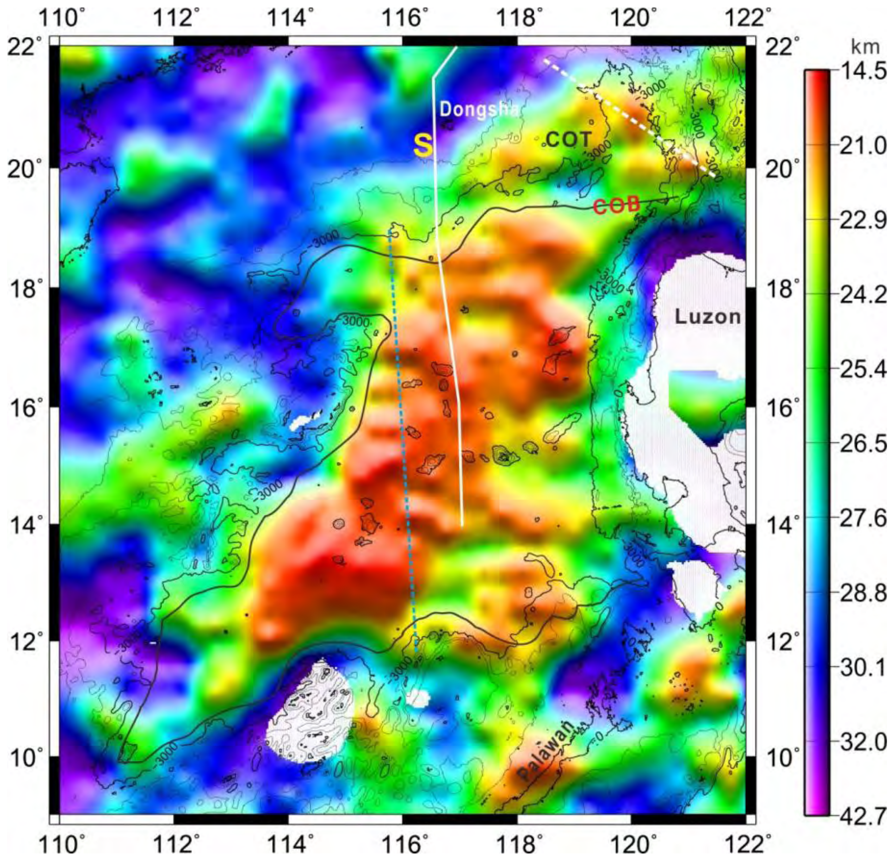

Figure 19 Map of Curie-point depths estimated from magnetic anomalies of the SCS assuming random 2D magnetization models. The white line marks the position of the reflection seismic line shown in Figure 21. COT = continent-ocean transition zone. See Figure 15 for other notations.

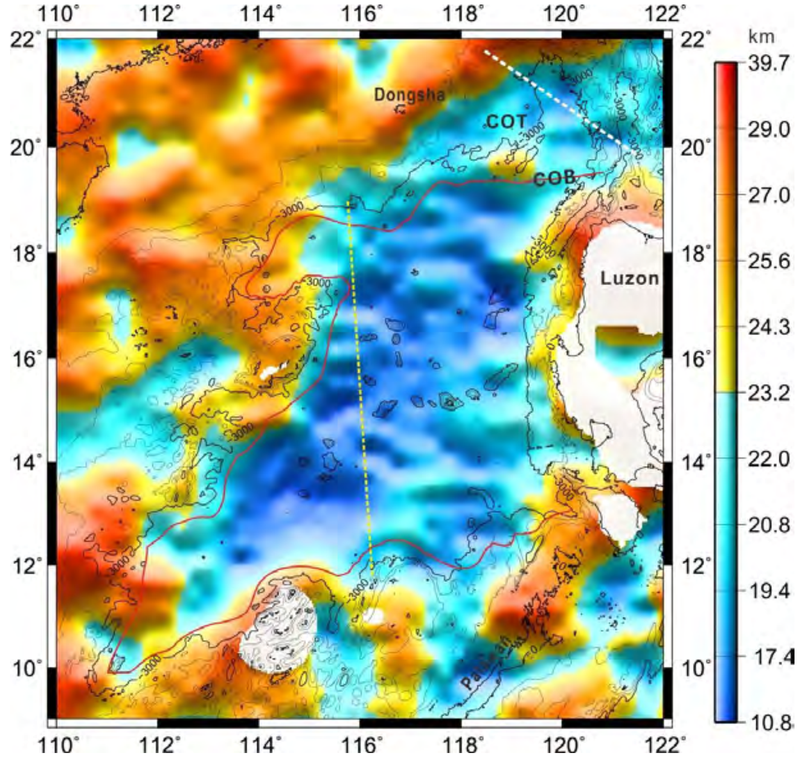

Figure 20 Map of thicknesses of the magnetic layer estimated from magnetic anomalies of the SCS assuming random 2D magnetization models. COT = continent-ocean transition zone.

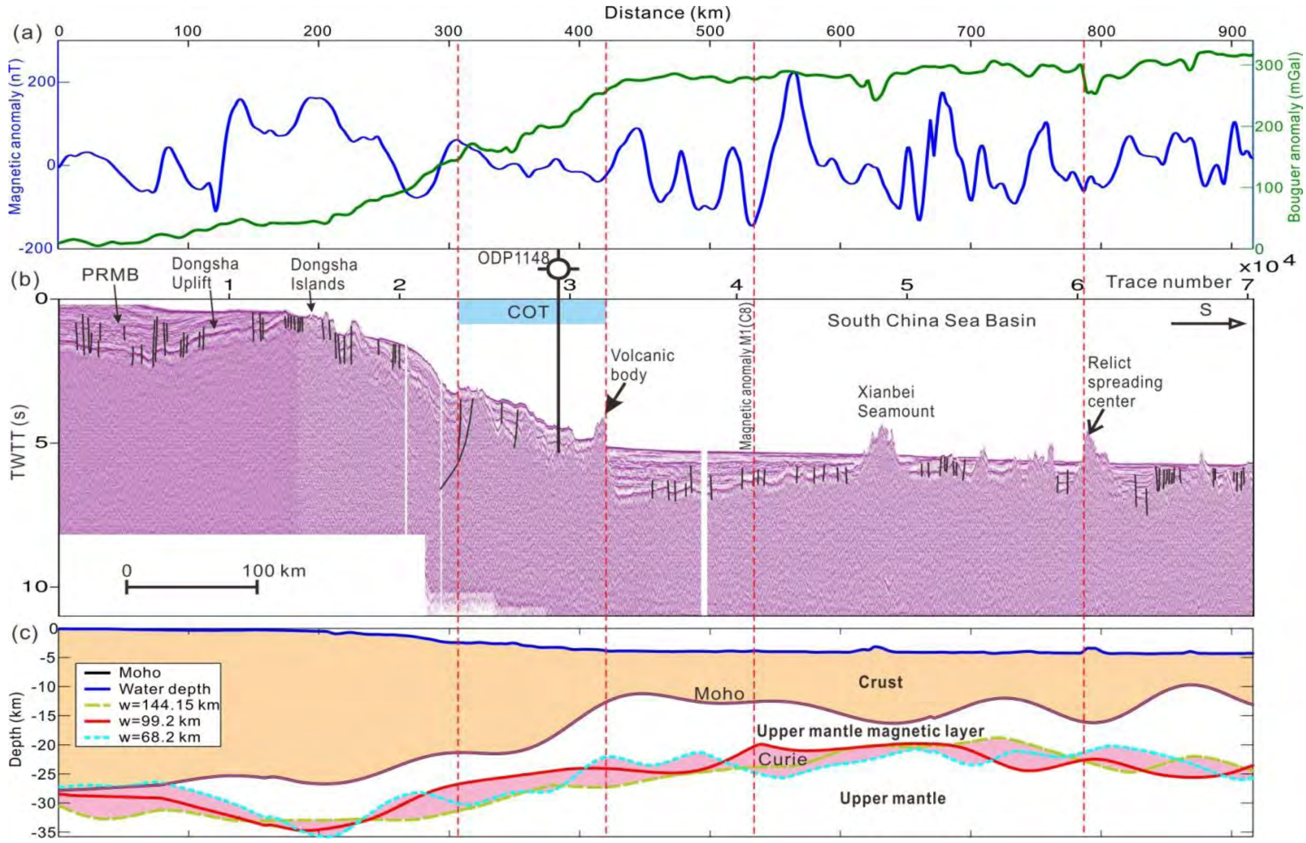

Figure 21 A regional geophysical profile in the SCS revealing magmatic activities, relationships between Curie and Moho depths, and key magnetic boundaries [Li et al., 2010]. It is seen clearly from this map that the magnetic quiet zone in the northern SCS continental margin coincides roughly to the COT there. TWTT = two-way travel time

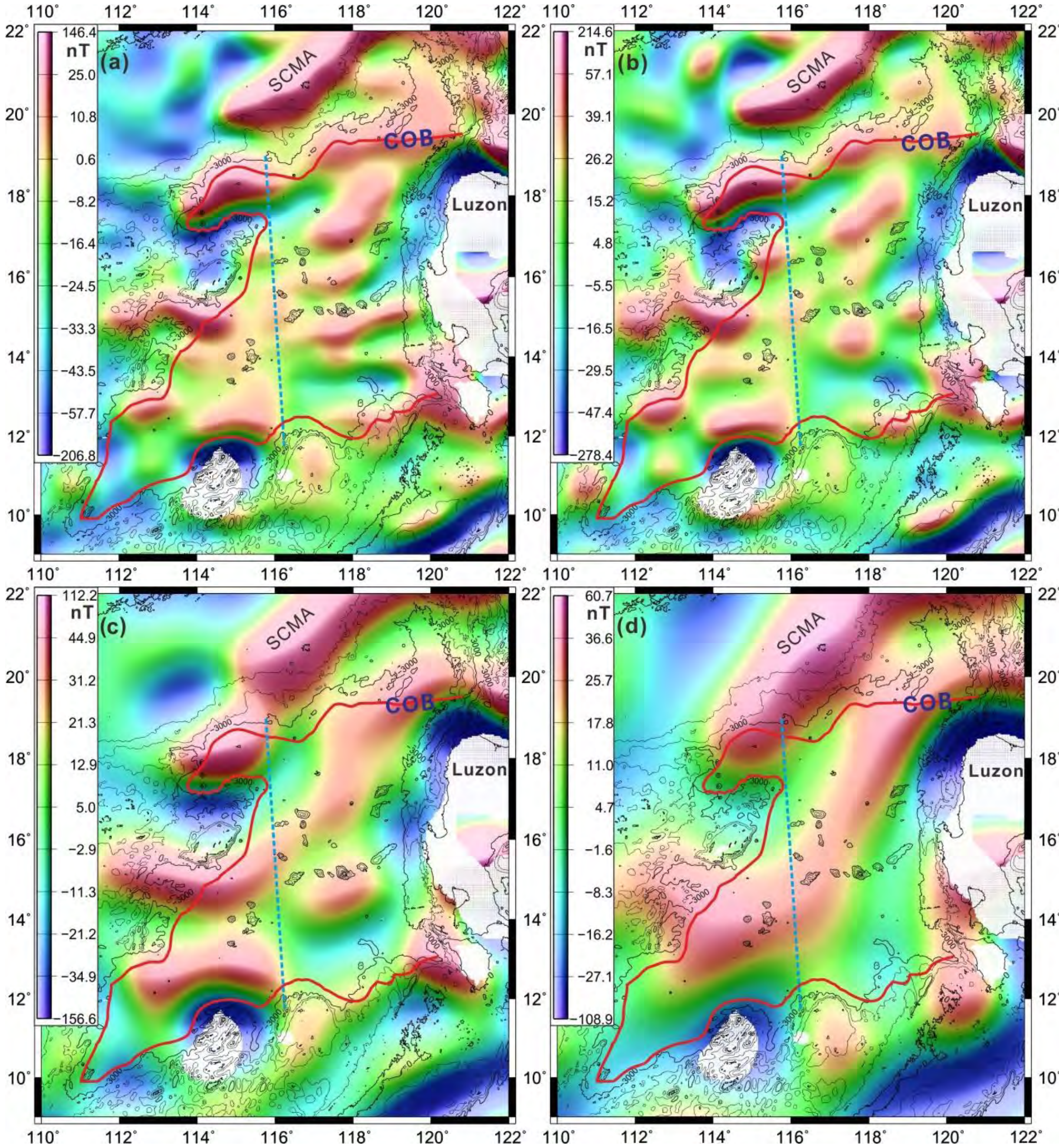

Figure 22 Maps of long-wavelength magnetic anomalies after filtering with 4 types of low-pass filters. (a) Using a Gaussian filter of 200 km wide in the space domain; (b) Using a low-pass filter with a 200 km cutoff wavelength; (c) Using a low-pass filter with a 300 km cutoff wavelength; (d) Using a low-pass filter with a 400 km cutoff wavelength. See Figure 15 for other notations.

On the magnetic quiet zone in the northern SCS continental margin

The so-called magnetic quiet zone (Fig. 24) in the northern SCS continental margin corresponds roughly to elevated Curie points and thinned magnetic layer, but since this zone is located within COT, it is conceptually very different from traditionally defined magnetic quiet zone developed within oceanic crusts. From integrated analyses of magnetic and reflection seismic data, we find that the area with very well preserved thick Mesozoic strata corresponds clearly with low 3D analytical signal amplitudes calculated from magnetic anomalies. Thick nonmagnetic Mesozoic strata can extend all the way to the COB, and their existence is the main cause for weak and quiet magnetic anomalies there. 3D analytical signal proves to be a very effective tool in detecting distributions of residue Mesozoic strata and late-stage magmatic bodies (Fig. 24).

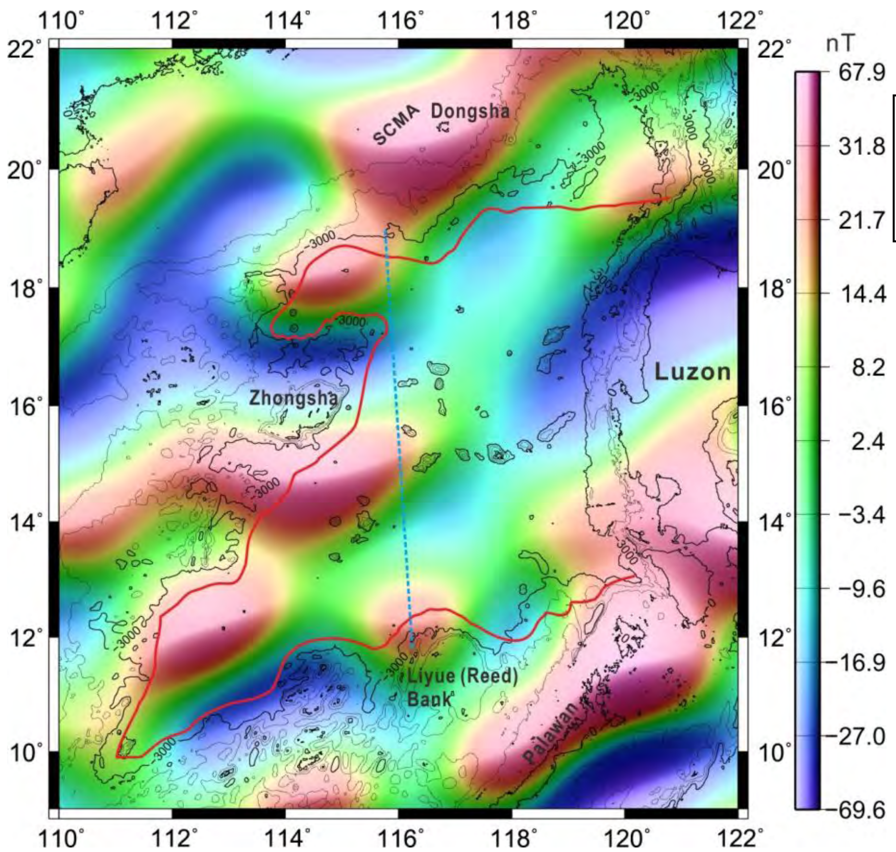

Figure 23 Regional map of satellite magnetic anomalies of the SCS. See Figure 15 for other notations.

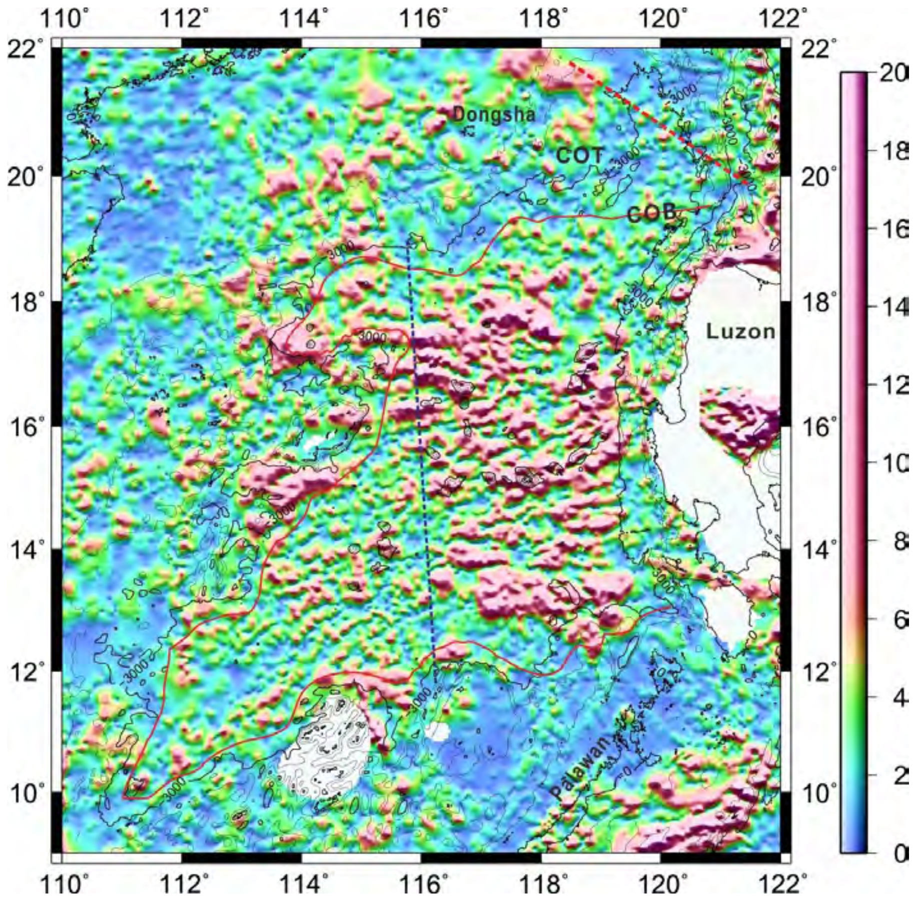

Figure 24 Regional Map of 3D analytical signal amplitudes calculated from regional air-borne and marine magnetic anomalies of the SCS. See Figure 15 for other notations.